



Particle tracking velocimetry as a method for chip ejection studies during groove milling of particleboard

Julius Hausmann¹ · Thomas E. Hafemann² · Frank Rüdiger² · Marcus Herzberg¹ · Christian Gottlöber¹

Received: 11 October 2022 / Accepted: 19 December 2022 / Published online: 12 January 2023
© The Author(s) 2023

Abstract

Studies on chip ejection from tools provide important information for the design of tools and effective chip collection elements used in woodworking machines. Among the chip properties, chip motion and its distribution are of particular interest for the design process. Until now, chip velocities have only been measured by manual tracking over a high-speed image sequence, which allows only a small scope of inspection. Here, we present the use of high-speed imaging in combination with particle tracking velocimetry as a new method for the semi-automatic evaluation of the magnitudes and directions of chip velocities. The methodology was tested in groove milling of particleboard. It was found that state-of-the-art particle tracking algorithms are suitable for quantitative analysis of chip motion in high-speed images. Therefore, spatial and temporal analysis of the chip velocity along the tool circumference are feasible and are presented here. In addition to chip velocity, chip collisions with the tool or other chips can be observed. This research also shows that image evaluation of chip sizes and shapes is potentially possible. In summary, the presented work provides methods that can quantitatively describe chip motion after chip formation. The experiments indicate that with each tooth engagement, new chips are formed, which initially move into the chip space at a median velocity higher than the cutting speed. After collisions with the tool and interparticle collisions, the particles leave the chip space of the tool at lower speeds. The machining tests performed with different process settings showed differences in the analysis results of chip movement. In the future, the presented methodology offers the possibility of investigating the relationships between tooth and chip space geometries, as well as different materials and the chip ejection of tools. Thus, the presented methodology provides a basis for creating a more general understanding of chip motion from machining operations, which can lead to innovations and improvements in chip collection.

1 Introduction

Understanding chip ejection from woodworking tools is crucial for the design of effective dust hoods. In today's furniture industry, a huge amount of energy is invested, to capture the chip and dust release from machining processes, both due to possible health impairment to workers and process disturbances in consequence of machine and work piece contamination (Lachenmayr and Kreimes 2006).

Owing to the high momentum of wood chips after chip ejection, chip collection often fails when the direction of the particle flow is not in line with the airflow of the removal

system. The higher the momentum of the chips, the more acceleration work must be done to change the flight direction of the chips. Chip guidance and redirection deflectors can be used to reduce chip momentum by redirecting and decelerating particles so that they can be more easily captured by the airflow in the hood (Heisel et al. 1999). However, the chip velocities and their spatial distribution must be known for the effective arrangement of these deflector elements. Therefore, it is important to investigate the velocity and mass distribution of chips after machining in order to design an effective collection hood. An improper collection hood design leads to poor energy efficiency. Improvements in design should, first, increase the total amount of chips and dust collected and, second, decrease the air flow rate required to remove dust and chips, resulting in lower energy requirements for the conveying system.

The spatial distribution of chips released from a cutting tool can be studied by using chip traps. A chip trap consists of specifically dimensioned chambers. The empty chip trap

✉ Julius Hausmann
julius.hausmann@tu-dresden.de

¹ Chair of Wood and Fibre Materials Technology, Technische Universität Dresden, 01062 Dresden, Germany

² Chair of Fluid Mechanics, Technische Universität Dresden, 01062 Dresden, Germany

is placed in a chip flow. After machining, the trap chambers are filled with chips and dust so that mass distribution, particle sizes and shapes, and ejection angles can be derived from the samples in the chambers (e.g. Fig. 1). However, determination of chip velocities is not possible with this method. The spatial resolution is limited by the size of the chambers. The significance of this test depends strongly on the overall quantity of collected chips, which in turn depends on the design of the chip trap and its positioning. The collection of dust particles is a challenge, due to their low sedimentation rate. Chip traps positioned close to the tool periphery will also affect the flow field of the tool and the occurring turbulence might affect the test results. Trials with chip traps were also performed by Heisel (2001).

Another way of visualizing the chip ejection is through infrared imaging. Due to internal and external friction, the temperature of machined material rises slightly. This temperature difference makes the particles stand out clearly from the ambient temperature, resulting in high-contrast images (Fig. 2). Depending on the image frequency and

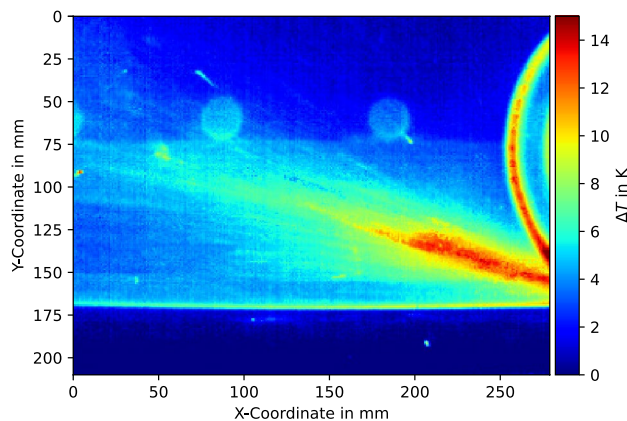


Fig. 2 Infrared image of the chip ejection in a machining test with the groove milling cutter Leitz No. 020161 and depth of cut $a_e = 2.5$ mm, feed speed $v_f = 15 \frac{m}{min}$ and rotational speed $n = 6000 \frac{1}{min}$ with an infrared camera (InfraTec VariaCAM, InfraTec GmbH, Dresden, Germany) with an image frequency of 50 Hz. The image shows the temperature difference of the particles to the ambient temperature. Particles are emitted from the tool (right picture side) and move towards the left side of the image

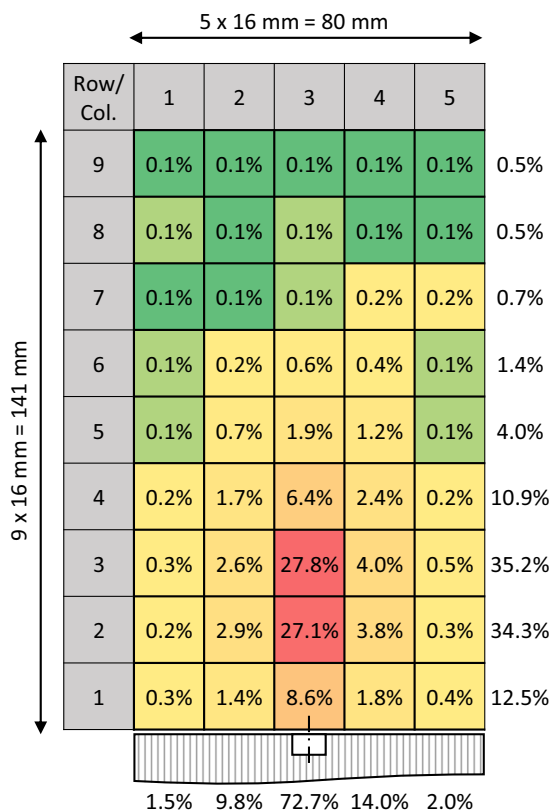


Fig. 1 Percentage mass distribution of the chips released in a machining test with the groove milling cutter Leitz No. 020161 and depth of cut $a_e = 3.5$ mm, feed speed $v_f = 10 \frac{m}{min}$ and rotational speed $n = 6000 \frac{1}{min}$ determined with a chip trap. The chip trap was positioned perpendicular to the workpiece surface at a distance of 40 mm from the outer diameter of the tool. The total amount of chips collected was 75.6%. All values were rounded to one decimal place

integration setting of the infrared camera, a time-averaged impression of the chip ejection can be obtained. The extent to which temperature differences in the image can be used to infer the particle density or mass distribution in the chip flow has not yet been investigated.

Short-term image captures using analog or digital photography have been used for chip motion analysis. Due to the high chip velocities in woodworking, short exposure times are necessary to detect fast-moving individual objects. For the determination of chip velocity, a sequence of at least two consecutive images with a fixed time interval showing an individual object is required. The measurement of the chip displacement per time interval can be done manually or automated by algorithms.

Pahlitzsch and Sommer (1966) investigated the influence of the chip space shape on the chip flow of planer blade shafts. The chip removal process was investigated with a high frequency film camera. The work compared eight different chip space designs, which were trapezoidal or arc-shaped, with different radii of curvature. Barz and Münz (1967) investigated the chip ejection of rebate cutters during push cutting parallel to the grain of air dry beech (*Fagus sylvatica* Carst.) and spruce (*Picea abies* L.) with the help of short exposure photography.

Heisel (2001) manually determined the chip velocities during chip formation on two tools with different chip space designs for beech, spruce, particleboard and medium density fiberboard with high-speed imaging. Keßler (2020) investigated the chip space design and the tooth shape of saw blades on the chip release with a special optical unit and high speed imaging. The rotating optical unit allowed a

steady tracking of a particular tooth. Therefore, the trajectory of chips was analyzed over the complete residence in the chip space. In addition to the tool, the process parameters of feed rate, cutting speed and material were also varied. The machined material and the tool design showed a significant influence on the chip formation, the size of chips and the chip trajectories. The manually measured particle velocities in the chip space were sometimes significantly higher than the cutting speed of the tool and appeared to vary with respect to the average chip thickness.

From the cited literature, it is clear that the phenomenon of chip ejection is complex. Moreover, chip ejection cannot be considered as a constant property of a particular tool, but depends on the chip space design (Pahlitzsch and Sommer 1966; Heisel 2001), material (Heisel 2001; Keßler 2020) and process settings (Barz and Münz 1967). The studies show that high-speed images contain a multitude of information about the chip ejection. However, manual analysis in the aforementioned chip ejection studies allowed only a small number of investigations. To overcome this limitation, an automated approach for chip ejection analysis should be used. Therefore, this study deals with the determination of chip velocities using high-speed imaging in combination with particle tracking velocimetry (PTV). In fluid mechanics, PTV, also known as Lagrangian particle tracking (LPT), is commonly used for the determination of particle velocities. A PTV algorithm detects objects on images and tracks the objects through a time series. This study addresses whether PTV can be used as a method for analyzing chip motion from high-speed videos and what information this method can provide. The setup chosen for image acquisition, the image processing to eliminate edge and background effects, and the evaluation methodology developed are therefore described and discussed in detail. The methodology is tested on video recordings taken during grooving of particleboard in climb cutting mode. This setup was chosen because these saw-like tools have fairly simple cutting tooth geometry and provide good visual accessibility. In addition, groove milling in climb cutting mode of particleboard is known to be problematic in terms of chip collection (Tröger 2004).

2 Material and methods

2.1 Machining trials

The machining trials were carried out with dedicated experimental equipment (Fig. 3), which essentially consists of a feed unit and a universal milling unit (Homag UF 11, 3 kW, HOMAG Group AG, Schopfloch, Germany), both operated by a control unit to allow mutable process

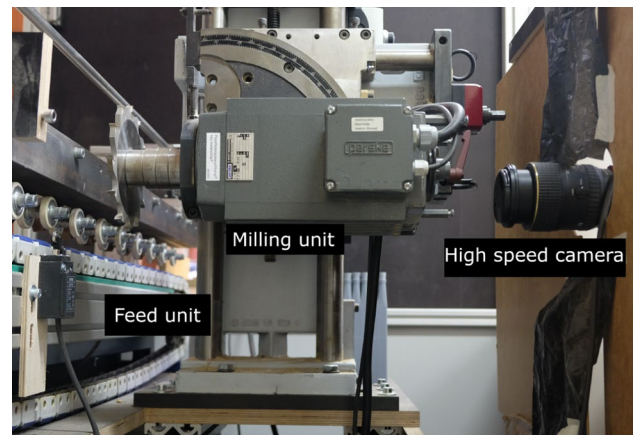


Fig. 3 Experimental setup for the machining trials. The image shows the feed unit, the milling unit and the high speed camera

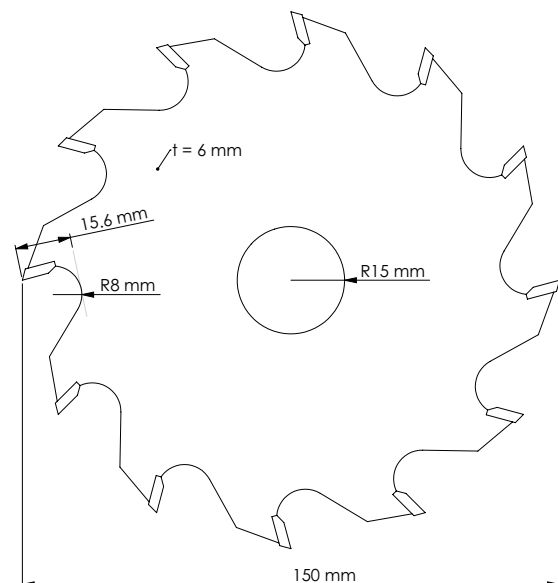


Fig. 4 Grooving Cutter Leitz GmbH Art. No. 020161

parameters. The installation is very similar to commonly used edge banding machines, but with better optical accessibility. The machining trials were conducted with 19 mm standard particleboard Type P2 E1 according to DIN EN 312:2010-12 (2010) and a standard grooving cutter (Art. 020161, Leitz GmbH & Co. KG, Oberkochen, Germany) with diameter of 150 mm, a cutting width of 8 mm and twelve teeth (Fig. 4). The process parameters of the trials (Table 1) were not selected with a typical industrial use case in mind. Instead, the rather low cutting velocities and the low depth of cut were selected to limit both particle velocity and particle concentration.

Table 1 Process parameters for conducted trials

Trial	Rotational speed	Feed speed	Depth of cut	Cutting speed	Average chip thickness
	n in $\frac{1}{\text{min}}$	v_f in $\frac{\text{m}}{\text{min}}$	a_c in mm	v_c in $\frac{\text{m}}{\text{s}}$	h_m in μm
1	6000	10	3.5	47.1	21.1
2	6000	10	8.0	47.1	31.8
3	9000	15	3.5	70.7	21.1

2.2 Image acquisition

The performance of PTV algorithms is limited by the frame-to-frame displacement of the particles as well as their concentration. The sampling theorem (Eq. 1) states that the frame to frame displacement of a particle f per time step δt should be less than half the smallest local spatial scale λ_{\min} (e.g. particle diameter) (Tropea et al. 2007). Another limiting factor of PTV is the minimal measurable displacement, which depends on how subpixel accuracy is modeled during image processing. Both the minimum and the maximum measurable displacement determine the possible dynamic range of the particle motion (Tropea et al. 2007).

$$f \delta t = \frac{1}{2} \lambda_{\min} \quad (1)$$

Wood machining is performed at high cutting velocities compared to metals and alloys. The particle sizes in the chip flow span a broad range from 1 μm to 1 cm. Assuming that the emitted particles will be accelerated to the cutting speed (see Table 1), the optimal sampling rate for PTV needs to be above the range of 100,000 frames per second (fps) regarding the sampling theorem (Eq. 1). Depending on the trajectories and particle density, PTV algorithms can still achieve good results well below this theoretical requirement if additional information is taken into account. For example, the position of a particle can be predicted by the displacement of previous frames, assuming smooth trajectories with no abrupt changes in acceleration. Therefore, the camera settings in this study were selected with the help of preliminary tests, where a compromise was found between the spatial and temporal resolution of the available camera gear and the tracking performance of the algorithm used.

All tests were carried out with the high speed camera Phantom VEO 410L (Vision Research Inc., Wayne, New Jersey, USA), positioned 50 cm from the cutting tool (Fig. 3). The videos were shot with 100 mm lens, aperture $f/5.4$ with ISO 8600 and an exposure time of 18.75 μs with a resolution of 256 pixels by 256 pixels, resulting in a frame rate of 57,000 $\frac{1}{\text{s}}$. The spatial resolution was about 80 $\frac{\mu\text{m}}{\text{px}}$, thus the image area was about 21 mm by 21 mm. An external

lighting panel, made from a LED strip, was attached to the test bench and provided a bright back light for the image acquisition. The camera was triggered by an electro-mechanical switch, when the work piece was in contact with the tool.

Because the covered image area was rather small compared to the size of the cutting tool, the camera was repositioned along the circumference of the cutting tool. The camera position was changed only in small steps, so that there was an overlap between the captured images of different positions. After repositioning the camera, the new position was determined by measurements from fixed reference points and an image calibration was performed. For calibration, a glass ruler was attached to the base body of the saw blade and the glass ruler was moved into the symmetry plane of the tool. After manual focusing and taking a reference image, the tool was moved back to the starting position, ensuring the focus was centered in the tools working plane. The focus depth at the chosen setting was about 14 mm.

In the test setup, the camera position was selected so that it is in the workpiece plane perpendicular to the feed direction. Therefore, the sawed groove and the particles in it are hidden laterally by the workpiece. To determine the particle velocity within the groove without influencing the cutting process itself, workpieces with pre-milled transverse grooves were used. The transverse grooves ran parallel to the camera orientation and had the same depth as the actual groove to be milled. Therefore, no machining was possible in the area of a transverse groove and chip flight could only be observed at a certain distance from the tool on the run-out side within the transverse groove.

Figure 5 shows exemplary video positions. Positions above the groove were numbered consecutively from “P1” to “P8” and the positions with transverse grooves were numbered “QN1” to “QN7”. Four unedited video sequences from different positions of the first machining test (Table 1) are available as supplementary information to this article.

2.3 Image pre-processing and data post-processing

The recorded scenes were converted into Audio Video Interleave format. The image pre-processing was performed with the open source software Fiji (Schindelin et al. 2012) and the tracking plugin TrackMate (Tinevez et al. 2017; Ershov et al. 2021). The first evaluation procedure consists of an image enhancement step and the tracking procedure. The image enhancement includes creating a mask of the cutting tooth and masking the original image (Fig. 6). This prevents particles from being incorrectly detected in the vicinity of the tooth. Afterwards, a background subtraction was performed with the rolling ball algorithm. The last step is a contrast enhancement

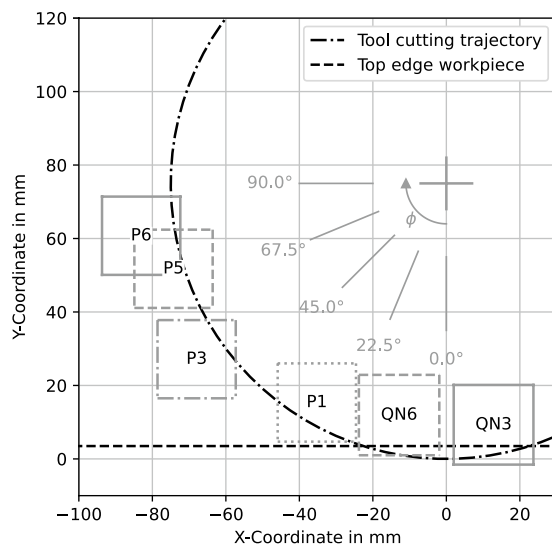


Fig. 5 Image detail of some video shots along the tool circumference

with the contrast limited adapted histogram equalisation (CLAHE) algorithm. Last, the image scale was added to the image meta data.

PTV was performed with TrackMate. The settings used are summarized in Table 2. For particle linking the “Linear motion LAP tracker” based on a Kalman-filter was used, as the particles move on highly linear trajectories with rather constant speed.

The image pre-processing and the actual tracking was automated with the Fiji API. The resulting trajectories, links and particle positions with all their attributes were saved in ASCII format for post-processing. For the analysis of the chip emission, the examination of the individual data sets is only suitable to a limited extent due to the small image area. Therefore, the local data sets were merged to a global data set via a coordinate transformation. The global data set was then subjected to further data processing by means of filters, calculation of missing variables and, finally, visualization of the test results. The described functionalities are provided by a dedicated object oriented class module in Python3 (Van Rossum and Drake 2009) based on Pandas (McKinney 2010) and Matplotlib (Hunter 2007).

For a reliable analysis of the particle tracks further filtering is necessary, to deal with the limitations of the linking algorithm. A high concentration of particles or intersecting trajectories can be erroneously linked. Since these cases would lead to higher deviations in the particle velocity and a decrease in the linearity of the particle, they are easily captured by the track filter (Table 2). The resulting particle trajectories can be further refined by a second set of filters, as done here.

Table 2 Settings of the particle tracking plugin TrackMate Version 7.7.2 (Tinevez et al. 2017)

Particle detection	
LoG-detector	
Threshold	0.05
Median filter	No
Subpixel accuracy	Yes
Particle filters	
Quality	> 2.8
Standard deviation intensity	< 17
Tracking	
Kalman-tracker	
Initial search radius	0.8 mm
Maximum search radius	1.5 mm
Gap closing	No
Track filters	
Linearity	> 0.9
Velocity standard deviation	< $5 \frac{\text{m}}{\text{s}}$
Minimum length	> 4 frames

Firstly the particles flight direction was used as a filter criterion. The chip movement is directed away from the tool (here in negative X-direction), therefore trajectories moving in the opposite direction (positive X-direction) must be false detections which are excluded from the evaluation. Secondly, the trajectories are filtered based on the statistic distribution of the trajectories ejection angle and the median velocity. In a local data set both values show approximately a unimodal, skewed distribution. Trajectories with feature values that did not fall within the range between $\bar{x} \pm 3\sigma$ were removed due to their low statistical feature probability, where \bar{x} is the median of a feature and σ is the standard deviation.

Data analysis showed that in some video scenes, the concentration of background particles had a significant effect on the resulting statistics. Background particles are defined as particles that do not originate from the cutting process of the tooth currently been in contact. In the final post-processing step, a Random-Forest-Classifer (Pedregosa et al. 2011) was trained on trajectory features to distinguish between foreground and background particles. The training set consisted of 473 sample tracks evenly selected from each video position and labeled according to three categories: “foreground”, “background” and “tool artifact”. The classifier object was initialized with the default parameters (scikit-learn 1.1.2) of 100 trees, no maximum depth, bootstrap sampling, and Gini impurity as a measure of the split quality. The training features were the track mean X and Y coordinates, track median speed, median ejection angle α , median contrast measure and median total intensity of the track spots, total distance

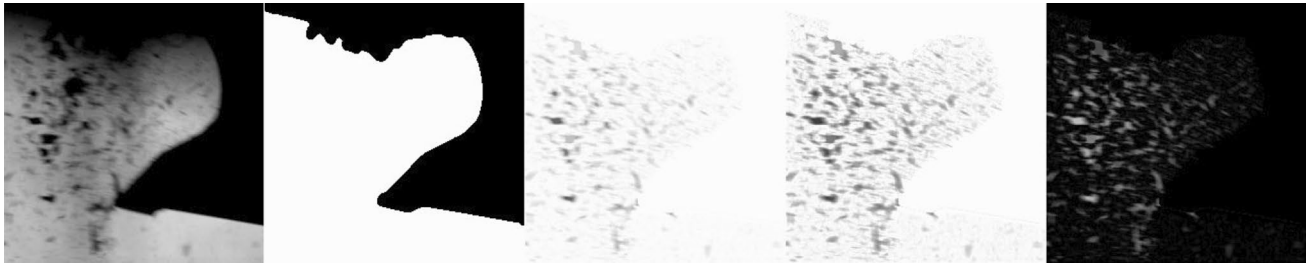


Fig. 6 Example of preprocessing steps (from left to right): raw image, tool mask, subtracted background and mask from raw image, CLAHE, inverted final image

traveled and ratio of the linear distance traveled and total distance traveled. The linear distance traveled is defined as the direct connection between the start and end point of one trajectory. The classification results were used as an additional filter for further data analysis and visualization. Table 3 shows the filter effect on the number of originally detected trajectories.

2.4 Analysis of particle size

In the second stage of the analysis, the relationship between the particle size and particle velocity, ejection

Table 3 Number of detected trajectories prior to additional filtering n_p and after filtering n_f for each machining trial (labels according to Table 1)

Trial no.	n_p in millions	n_f in millions	$1 - \frac{n_f}{n_p}$ in %
LoG-detector			
1	1.43	0.87	38.6
2	0.79	0.33	58.2
3	0.91	0.37	58.9
Mask-detector ^a			
1	0.108	0.033	69.7
2	0.058	0.019	66.2
3	0.038	0.018	53.8

^aOnly 1000 frames per video sequence were analyzed

Fig. 7 Example of image processing steps for particle analysis (from left to right): raw image, classified binary image, subtracted tool mask



angle, or the particles spatial distribution should be explored. Trackmate requires a segmented binary or grayscale image to determine the size and shape descriptors of particles. Therefore, the previously described image processing methodology could not be used. Segmentation via a classical threshold method proved to be challenging, because the contrast between particles and the background differs significantly from scene to scene. Therefore, a random forest classifier of the ilastik framework (Berg et al. 2019) was used for segmentation. The classifier was trained with the features “Gaussian smoothing”, “Laplacian of Gaussian”, “Gaussian Gradient Magnitude”, “Hessian of Gaussian Eigenvalues” with kernel sizes of 0.7 px; 1.6 px and 5.0 px. Using manual markers on training images, the classifier learns the division into foreground and background pixels. The segmentation results were exported and saved as binary images (Fig. 7). Particle tracking was performed using Trackmate. The same settings were used as before, only the algorithm for particle detection was changed to “Mask-Detector”. The Mask-Detector module then automatically provides the particle analysis data for each point in a trajectory.

The particle area can differ significantly along a trajectory because of overlap with other particles or particle rotation. This leads to different size and shape measurements of the same particle in the different video images. For further analysis, the median of these measurement values was assigned to the trajectory as a property.

3 Results and discussion

3.1 Particle properties determined with PTV

Observations of individual film recordings clearly show that chip ejection is a periodic phenomenon determined by the cutting frequency of the teeth. Figure 8 shows the total count of particles detected during particle tracking for each frame over time before further filtering, visualizing the periodic nature of the chip emission. The dominant frequency, determined from the Fourier-transformed signal (Fig. 8 bottom), matches the nominal cutting frequency of 1200 Hz closely. With each tooth engagement, new chips are formed over the cut length, which initially move into the chip space of the tool in a relatively directed manner and then leave this space

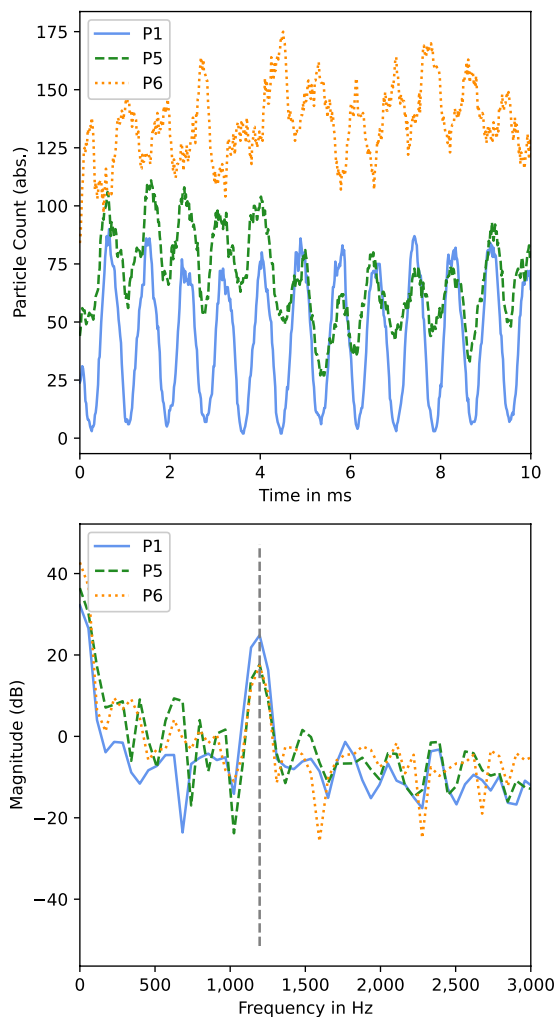


Fig. 8 Number of detected particles per frame over a period of 20 ms for different video positions captured during machining of particleboard with $n = 6000 \frac{1}{\text{min}}$, $a_e = 3.5 \text{ mm}$ and $v_f = 10 \frac{\text{m}}{\text{min}}$. Raw data from particle tracking without further filtering

after renewed contact with the tool in a more dispersed manner. During each chip ejection, some particles travel ahead of the main trail of the chips at high speeds. The main trail of the chips consists of particles moving at a similar speed, followed by slower particles. The video position near the cutting point shows almost exclusively particles originating from the immediate tooth engagement. Along the cutting trajectory with increasing distance to the cutting point, an increasing number of smaller particles can be observed in the recordings, which move significantly slower than the ejected particles and do not originate from the current tooth engagement. Additionally, it is shown that video positions farther away from the cutting point have a higher concentration of background particles, as the total count of particles between two engagements does not reach values close to 0 and is offset by an almost constant value (see Figs. 5, 8).

The global data set allowed the visualization of the overall particle emissions in a vector plot. Therefore, the global investigation area was divided in grid like subareas (spatial binning) and all links were grouped by their specific subarea. The medians of the particle velocity and ejection angle were used to create the vector plot in Fig. 9.

Chip formation occurs in the area with a positive X-coordinate (Fig. 9). The highest median particle velocity can be found in the area of chip formation with values close to $60 \frac{\text{m}}{\text{s}}$ and is therefore higher than the nominal cutting velocity of $47.7 \frac{\text{m}}{\text{s}}$, which supports the observations by Keßler (2020) and Heisel (2001). The particle trajectories are directed to the inside of the chip space. For the area with X-coordinates between -40 mm to 0 mm , the chip trajectories run trough the chip space. The median particle velocity decreases to values between $40 \frac{\text{m}}{\text{s}}$ to $50 \frac{\text{m}}{\text{s}}$ due to collisions with the tool

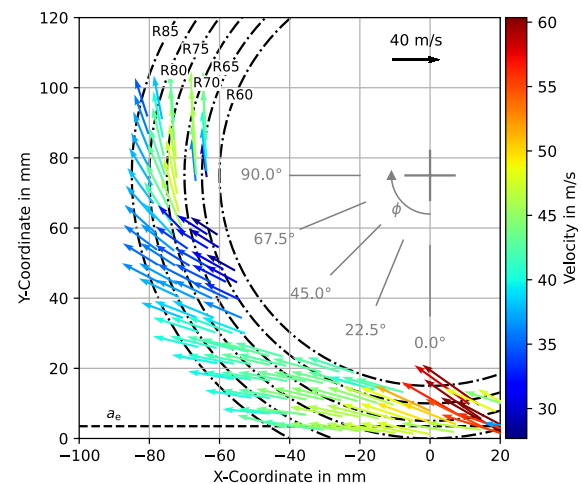


Fig. 9 Visualization of the median particle velocity. Global data set for machining of particleboard with $n = 6000 \frac{1}{\text{min}}$, $a_e = 3.5 \text{ mm}$ and $v_f = 10 \frac{\text{m}}{\text{min}}$. The circumference of the tool is labeled with “R75”, where “R60” is close to the circumference of the deepest point of the tools chip space. The line labeled as a_e is equal to the top of the work piece

and particle-particle collisions. Following the tools cutting trajectory, the particles median velocity further decreases to values between $30 \frac{\text{m}}{\text{s}}$ to $40 \frac{\text{m}}{\text{s}}$ and then increases again for Y-coordinates $> 75 \text{ mm}$.

Figure 10 shows the velocity magnitudes (a) and directions (b) of the particles inside the chip space along the

radius $R = 70 \text{ mm}$ (see Fig. 9) for all three trials. The values are plotted over the tools angle of rotation ϕ . The cut angle ϕ_c is the inclined angle between angles of rotation ϕ from -17.57° to 0° for the first and third trial and between -26.70° to 0° for the second trial. The chips flight direction is defined as the inclined angle α between the chip trajectory and the horizontal axis.

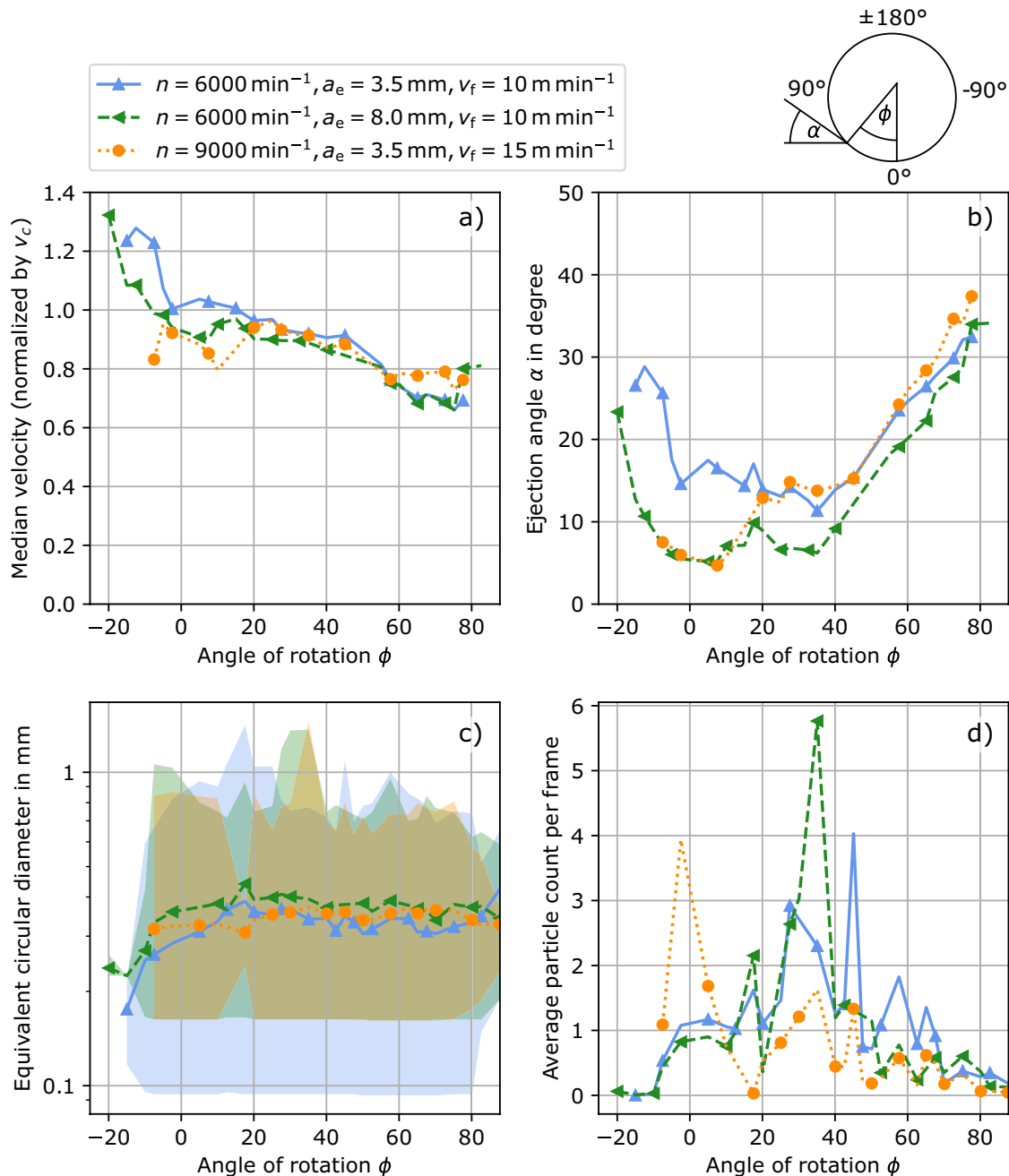


Fig. 10 Visualization of the median particle velocity (a), particle ejection angles (b), particle size (c) and particle concentration (d) within the chip space over the tools angle of rotation. Evaluation along an arc with radius 70 mm to the rotational axis of the tool. The

data shown in c were obtained from the analysis of binary images with the mask-detector. The shaded area around each line indicates the range of minimum and maximum particle sizes

To simplify the comparison, the median velocity was normalized by the nominal cutting speed of each test. The velocity magnitudes show minor differences for the three trials with the highest values in the region of the chip formation. The median particle velocity then continuously decreases for higher angles of rotation, as described before. The median ejection angles differ significantly among the three trials. During chip formation the chips flew at a 10° smaller ejection angle for the trial with a rotational speed of $6000 \frac{1}{\text{min}}$ and a depth of cut of 8.0 mm compared to the trial with 3.5 mm depth of cut. For angles of rotation greater than 10° , the difference between the ejection angles for both trials becomes smaller; however, the particle ejection angles are flatter in this range for the trial with an 8.0 mm depth of cut. The ejection angles for the trial with a rotational speed of $9000 \frac{1}{\text{min}}$ and a depth of cut of 3.5 mm lie between those of the other two trials. In the area of chip formation, the values are closer to the experiment with 8.0 mm depth of cut, whereas in the range of higher angles of rotation, the values match the trial with 3.5 mm depth of cut.

Figure 10c shows the mean particle size over the angle of rotation. The minimum particle size is $80 \mu\text{m}$ and $160 \mu\text{m}$ respectively over all angles of rotation, which is close to the minimal resolution of the camera system used. The maximum particle size decreases with an increase in the rotation angle and is quite similar for all three trials. The mean particle size increases to angles of rotation of up to 20° and then slightly decreases again for all three machining trials. The experiment with a depth of cut of $a_e = 8 \text{ mm}$ resulted in a slightly coarser particle distribution on average, which can be explained by a higher average chip thickness and a larger cutting angle as well as a deeper cut into the middle layer of the particleboard, which consists of coarser particles.

Figure 10d shows the average number of particles per frame over the angle of rotation. The maximum particle concentration is reached during an angle of rotation between 25° to 50° for both experiments with rotational speed $n = 6000 \frac{1}{\text{min}}$. In this range, the chips leave the chip space, which they enter after the chip formation. Even though these results are strongly affected by the applied filters and remaining background particles, the position of the maximum concentration is in rough agreement with both the temperature maximum in the thermogram (Fig. 2) and the maximum mass captured with the chip trap (Fig. 1).

One reason for the smaller measured ejection angles (Fig. 10b) in the second test compared with the first could be the larger cutting angle ϕ_c . By definition, the cut ends at the tool rotation angle of $\phi = 0^\circ$. The cutting angles ϕ_c of the experiments show in comparison that cutting starts

earlier in the second test. Consequently, the chips collided and deflected at an earlier time in the deepest point of the chip space. Assuming that the angles of impact and rebound in the chip space remain the same for all particles in the rotating tool reference system, a smaller ejection angle α results for the absolute reference system. However, because the chip thicknesses of the two tests also differed, this assumption may not be justified.

The setting variables of the cutting process and the three-layered structure of the particleboard could also be of significance for the smaller observed ejection angles. As described above, coarser chips were formed in the second trial (Fig. 10c), which therefore also have a greater mass. Owing to their greater mass, these particles experience a greater centripetal force or acceleration in the radial direction, which could also lead to smaller ejection angles α relative to the selected reference frame. Centripetal force could also be a reason why the ejection angles observed in the third trial were smaller for small angles of rotation compared with the first trial. Here, the mass should be the same, but the angular velocity is higher, leading to an increase in the radial acceleration.

3.2 Methodological influences

The described experiments and measurements are subject to physical and methodological influences, which limit the accuracy of the results. Real chip emission is a three-dimensional problem, which was only considered in two dimensions in this investigation using image acquisition. Neglecting the velocity component in the depth direction of the image plane systematically leads to a lower observed particle velocity. Other investigation methods can be used to estimate this error. Our investigations using a chip trap and infrared camera indicate that the chip emission propagates symmetrically with respect to the plane of the tool blade at an angle of $\pm 4^\circ$, leading to a maximum error of 7% for velocity magnitude. Therefore, in this case, a two-dimensional consideration of chipping appears to be permissible.

The overall accuracy of digital image acquisition depends on sensor design, lens accuracy, calibration accuracy, and other factors. Exposure in conjunction with exposure time also affects the accuracy of image information. Image acquisition under backlight conditions, where more light is scattered toward the sensor, results in less sharp particle contours or weaker intensity gradients, leading to a lower signal-to-noise ratio. This can have a significant impact on the detection of smaller particles. In the present case, the particle size distribution spans a wide range, and the optical resolution of $80 \mu\text{m}$ is already larger than the particle diameter of some particles in the size distribution. The results shown therefore only reflect particles with a diameter $> 200 \mu\text{m}$. This applies both to the evaluation with the

LoG-detector from the grayscale images and to the evaluation of the binary images with the mask-detector.

The analysis of binary images to determine the particle size is subject to further limitations resulting from the setup. The movement of the particles through the static image section causes them to be cropped at the edges. Particles that touch the edge of the image must be excluded from the evaluation because the part outside the image section is unknown. The probability that a particle is cut off from the image edge at a random center position increases when the particle dimension approaches the size of the image field. Following ISO 13322-2:2021-12 (2021), this effect can be considered by an edge error correction, but is not applied here, because here not only the image edge but also the moving tool leads to an edge effect that can hardly be considered practically. As the center position of the particles is not random but depends on the camera position with respect to the tool, a systematic discrimination of particles can occur. In terms of tracking, it is also true that larger particles have a higher probability of overlapping with other particles. If particle overlapping occurs in successive images, this leads to a sudden change in the centroid of the area, and thus to an incorrect calculation of the particle displacement. In addition, the standard deviation of the particle area along the trajectory increases. Both criteria were used as filters to detect and exclude the erroneous trajectories. As a result, larger particles are underrepresented in the particle size analysis. Considering the methodological problems mentioned above, only basic information can therefore be obtained from the presented size analysis. A spatially resolved investigation of chip size using chip traps represents a more robust method, that should be used as an alternative for future investigations.

Finally, the influence of the filters during data processing should be mentioned, which should systematically suppress disturbing effects. The filters developed are necessary for a representation of the active chip emission, because the large number of small dust particles and incorrectly detected trajectories have a significant influence on the statistics shown. The filter criteria therefore represent a significant influence on the results and were critically examined. However, the determination of the filter criteria or the selection of training data for the classifier remains partly a result of subjective assessment.

4 Conclusion and outlook

The results presented show that with current high-speed cameras and particle tracking algorithms, semi-automatic evaluation of tool chip emission with statistically large sample numbers is possible. For image acquisition, a compromise must be found between the required frame rate and the image resolution for evaluation using PTV. Erroneously

detected trajectories and a high number of background particles necessitate the use of filters that can be generated manually or by machine learning. Combining multiple image positions provides the ability to perform a spatial and temporal analysis of the magnitude and direction of chip velocity in the flight sector. Additional information such as chip concentration or chip size can be evaluated to a limited extent. The range of chip size analysis is determined by the image resolution. A large error influence on the chip size analysis represents the superposition of particles. The determination of the spatial chip concentration is influenced by the accumulation of dust particles in the experimental environment, or by the filter used to suppress these particles in the evaluation.

The evaluation of the machining trials shows that chip ejection is a periodic phenomenon determined by the cutting frequency of the cutting teeth. Formed chips initially move into the chip space with a median velocity higher than the actual cutting speed. After renewed contact with the tool, the particles leave the chip space of the tool with reduced particle velocity. From the results of the three tests, it can be observed that the process parameters influence the chip ejection of the tool. However, further experiments are necessary to qualitatively or quantitatively describe the effects of the individual process parameters.

As the presented study was limited to the analysis of groove milling as a machining process and particleboard as a material, other manufacturing processes and materials should be investigated in the future, to extend the current state of knowledge.

Chip ejection studies (Pahlitzsch and Sommer 1966; Keßler 2020; Heisel 2001) indicate that tooth geometry, machining material and chip space design have a significant influence on the chip emission of a tool. Therefore, future investigations should focus on the identification of influencing factors in tool design for the targeted manipulation of chip emissions to achieve a functional improvement in hood design in machining situations with low degrees of chip collection. Numerical simulation methods, such as the discrete element method (DEM), may be able to calculate chip ejection and eliminate the need for experiments. However, validation data is required for the development of these simulation models. Therefore, the presented work contributes to these developments with the obtained data, as well as with the tested methodology.

Supplementary Information The online version contains supplementary material available at <https://doi.org/10.1007/s00107-022-01917-0>.

Author contributions JH participated in the experiments, conducted the data pre- and post-processing, wrote the manuscript and created figures and tables. TEH participated in the experiments and gave notes on data analysis and data visualization. CG supported the literature research and revised the manuscript. MH supported the planning and construction of the test rig. FR has supported the high-speed video

imaging and particle tracking and contributed to the writing of the manuscript. CG and FR took over the coordination of the project. All authors reviewed the final manuscript.

Funding Open Access funding enabled and organized by Projekt DEAL. The research project IGF No. 20598 “Experimentelle Untersuchung und numerische Modellierung der Spanerfassung beim Nutsägen bzw. -fräsen von Holzwerkstoffen als Grundlage für deren Optimierung”, was supported by the Federal Ministry of Economic Affairs and Climate Action through the German Federation of Industrial Research Associations (AiF) as part of the program for promoting industrial cooperative research (IGF) on the basis of a decision by the German Bundestag.

Availability of data and materials Data available on request.

Code availability Not applicable.

Declarations

Conflict of interest All authors declare that they have no conflicts of interest.

Ethics approval Not applicable.

Consent to participate Not applicable.

Consent for publication Not applicable.

Open Access This article is licensed under a Creative Commons Attribution 4.0 International License, which permits use, sharing, adaptation, distribution and reproduction in any medium or format, as long as you give appropriate credit to the original author(s) and the source, provide a link to the Creative Commons licence, and indicate if changes were made. The images or other third party material in this article are included in the article's Creative Commons licence, unless indicated otherwise in a credit line to the material. If material is not included in the article's Creative Commons licence and your intended use is not permitted by statutory regulation or exceeds the permitted use, you will need to obtain permission directly from the copyright holder. To view a copy of this licence, visit <http://creativecommons.org/licenses/by/4.0/>.

References

- Barz E, Münz UV (1967) Der Spanablauf bei Fräsen für die Holzbearbeitung (The chip flow in milling cutters for wood machining). *Holz Roh- Werkst* 23(11):422–428
- Berg S, Kutra D, Kroeger T et al (2019) ilastik: interactive machine learning for (bio)image analysis. *Nat Methods*. <https://doi.org/10.1038/s41592-019-0582-9>
- DIN EN 312:2010-12 (2010) Spanplatten - Anforderungen; Deutsche Fassung EN 312:2010 (particleboards—specifications; German version). Norm, Deutsches Institut für Normung e. V., Berlin, Germany
- Ershov D, Phan MS, Pylvänäinen JW et al (2021) Bringing trackmate in the era of machine-learning and deep-learning. *Biorxiv*. <https://doi.org/10.1038/s41592-022-01507-1>
- Heisel U (2001) Auslegung von Absaughauben bezüglich der Späneerfassung durch Simulationsrechnung: BMWi/ AiF- Nr. 12311: Abschlussbericht (Design of exhaust hoods with respect to chip collection by simulation: BMWi/ AiF- Nr. 12311: Final Report)
- Heisel U, Tröger J, Haag M et al (1999) Spänestrahle gezielt leiten: Neue Wege zur Verbesserung der Späneerfassung in Holzbearbeitungsmaschinen (1) (Directing the chip flow in a targeted manner: New ways to improve chip collection in woodworking machines (1)). *HK Holz- und Kunststoffverarbeitung* 34(7–8):74–76
- Hunter JD (2007) Matplotlib: a 2d graphics environment. *Comput Sci Eng* 9(3):90–95. <https://doi.org/10.1109/MCSE.2007.55>
- ISO 13322-2:2021-12 (2021) Particle size analysis—Image analysis methods—part 2: dynamic image analysis methods. Standard, International Organization for Standardization, Geneva
- Keßler R (2020) Detektion und Auswertung der realen Spantenstehung und Dynamik bei der Holzbearbeitung mittels Kreissägewerkzeugen und deren Optimierung als Konditionierung zur ganzheitlichen Späneerfassung: BMWi/ AiF- Nr. 19422: Abschlussbericht (Detection and evaluation of real chip formation and dynamics in woodworking by means of circular cutting tools and their optimization as conditioning for holistic chip detection: BMWi/ AiF- Nr. 19422: final report)
- Lachenmayr G, Kreimes H (2006) *Energietechnik für die Holzindustrie (Energy technology for the wood industry)*, 3rd edn. Retru-Verlag e.K., Weyarn
- McKinney W (2010) Data structures for statistical computing in python. In: *Proceedings of the 9th Python in science conference*, Austin, TX, pp 51–56
- Pahlitzsch G, Sommer I (1966) Erzeugung von Holzschneidspänen mit einem Messerwellen-Spaner - Vierte Mitteilung: Spanraumform auf Spanbildung und Spanablauf: Einfluß der Spanraumform auf Spanbildung und Spanablauf (Production of wood-cutting chips with a chip flaker - Fourth report: Influence of chip space shape on chip formation and chip flow). *Holz Roh- Werkst* 24(6):260–269
- Pedregosa F, Varoquaux G, Gramfort A et al (2011) Scikit-learn: machine learning in Python. *J Mach Learn Res* 12:2825–2830
- Schindelin J, Arganda-Carreras I, Frise E et al (2012) Fiji: an open-source platform for biological-image analysis. *Nat Methods* 9(7):676–682
- Tinevez JY, Perry N, Schindelin J et al (2017) Trackmate: an open and extensible platform for single-particle tracking. *Methods* 115:80–90. <https://doi.org/10.1016/j.ymeth.2016.09.016>
- Tröger J (2004) Lösungsansätze zur Späneerfassung in Hochleistungsbearbeitungszentren (Solutions for chip detection in high-performance machining centers). In: *Annals of Warsaw Agricultural University—SGGW, Forestry and Wood Technology*, vol 55. Warsaw University of Life Sciences, pp 560–568
- Tropea C, Yarin A, Foss J (2007) *Springer handbook of experimental fluid mechanics*. Springer, Berlin
- Van Rossum G, Drake FL (2009) *Python 3 reference manual*. CreateSpace, Scotts Valley

Publisher's Note Springer Nature remains neutral with regard to jurisdictional claims in published maps and institutional affiliations.